Theoretical study of the pressure-induced structural phase transition of VO_2

Yulong Wang,[1] Zhenyi Jiang,[1,*] Xiaodong Zhang,[1] Jiming Zheng,[1] and Aijun Du[2,*]

[1]*Shaanxi Key Laboratory for Theoretical Physics Frontiers, Institute of Modern Physics, Northwest University, Xi'an 710069, China*

[2]*Centre for Materials Science, School of Chemistry and Physics, Science and Engineering Faculty, Queensland University of Technology, Gardens Point Campus, Brisbane QLD 4001, Australia*

(Received 9 May 2023; revised 19 July 2023; accepted 11 August 2023; published 23 August 2023)

High pressure technology is an effective method for studying whether there is Mott or Peierls phase transition (PT) from insulator to metal phase. It is unclear whether there is a Mott or Peierls PT in the ambient M1/R → the high-pressure X phase for bulk VO_2. Based on first-principles calculation, insulator M1 → semimetallic X and metallic R → semimetallic X PT path were studied. During the pressurization of the ambient M1 phase, it will transform into two nearly degenerate intermediate phases of M1′ and M1″. The M1″ phase has a significantly lower band gap (no zero band gap) owing to its relatively longer length of V-V V-V shorter bond and V-O bond. The M1″ → X path is the more probable route owing to its lower potential barrier and shorter moving route of V atoms relative to those of M1′ → X path. Those V atoms at the (002) crystal plane of crystal cell will shuffle nearly along the [100] crystal direction as volume pressurization in the M1″ → X path, while the averaging of V-V spacing occur and the band gap gradually decreases to zero or even a negative value. Uniaxial stressing of the metal R phase along [100] or [010] crystal direction leads to the $CaCl_2$-type orthogonal metal phase (O phase, space group No. 58, *Pnnm*). Upon cooling the O phase under high pressure, it will transform to M1″ and then the X phase. Those V atoms at the (002) crystal plane of crystal cell continuously shuffle along the [10-1] crystal direction in the O → M1″ path, moreover the difference in longer and shorter V-V bond lengths tends to increase and a new dimerization of the V-V dimers appears. The PT paths from the semiconductor M1 → semiconductor M1″ → semimetal X phase and from metal R → metal O phase only involve geometrically structural PT. Especially, it is a typical reconstruction-type and martensiticlike PT, and no PT of electronic structure from semiconductor to metal phase is involved in the path from semiconductor M1″ → semimetal X phase. The structural PT path from metal O → semiconductor M1″ phase is a typical Peierls PT or pseudo Mott PT within our DFT+U calculations even though the Coulomb repulsion between electrons is always present and works. The Coulomb repulsion between electrons cannot cause the electronic structural PT to happen properly.

DOI: 10.1103/PhysRevB.108.064105

I. INTRODUCTION

Vanadium dioxide (VO_2), as a prototype of strongly correlated electron materials, has been paid attention in the condensed matter physics and material sciences for several decades [1]. The electron correlation interplaying with lattice can stabilize a very rich phase diagram of VO_2 that consists of many phases with distinct structures and electronic properties. The PT between these phases can be driven by temperature, hydrostatic pressure, uniaxial stress, photoexcitation, and electrical gating [1–4]. For example, the well-known, insulating M1 (monoclinic, space group $P2_1/c$) phase can reversibly transform to the metallic R (tetragonal, $P4_2/mnm$) phase at approximately 340 K under ambient pressure upon heating [1], in which the first-order structural PT and metal-insulator PT always occur simultaneously. Because of a delicate interplay between crystal structure and electronic correlation occurs during the PT, the driving force behind PT still remains unclear and has been a topic of controversy. Based on experimental observation, an electron-correlation-driven Mott transition [5–10], and a structurally distortion-driven Peierls transition [11–18] were proposed to try to understand the PT. And now most studies [19–25] suggested that the cooperation of Mott correlation and Peierls distortion play an important role in the PT at the same time.

The application of external pressure provides a unique way to investigate the relationship between structural and electronic properties. Hydrostatic pressure applied via a diamond anvil cell has also been able to drive the M1 phase to another isostructural and more conductive M1′ and M1″ phase [26–31] above 12 GPa, and finally to a so-called metallic X (monoclinic) phase above approximately 34 GPa at room temperature [28,30–32]. The new phase X can be indexed on a monoclinic unit cell of baddeleyitelike structure [28]. In addition, the high-temperature metallic R phase can also be pressed to be an open metallic O phase above 14 GPa and then X phase above 38 GPa at 383 K [28,31].

Previous experimental work [27,33,34] to study the driving force in the pressure-induced PT reported the strong enhancement of metallicity within the M1′ phase and supported a major role of the electron correlations (Mott-Hubbard) against charge-lattice coupling. Subsequent study [28] assumed that the metallization can only appear in the phase X under high

*Corresponding author: jiangzy@nwu.edu.cn

pressure. The pressure-induced metal-insulator PT from M1 to X phase should be driven by a structural PT. Recent experimental studies [30] suggested that the pressure-induced PT from M1 to M1′ phase is associated with electron-electron correlations, while the PT from M1′ to X phases is related to structural PT.

Despite previous studies, the abovementioned have discovered the cooperation of Mott correlation and Peierls distortion, however, under the premise without the PT path, it is impossible to infer which one of electron-correlation-driven Mott transition and a structurally distortion-driven Peierls transition plays a major role in the pressure-induced metal-insulator phase transition (MIT).

In this paper, based on the density functional theory (DFT) with Dudarev implementation (DFT+U) [35], the gradual evolutions of the V-V spacing, PT path, and energy band were studied from M1 to X phase, and from R to O, then to X phase in the pressure induced PT. We found that during the PT from M1″ to X phase, only the band gap decreases gradually, and with the reconstruction of chemical bond between atoms. It is a typical reconstruction-type and martensiticlike PT, and no PT of electronic structure from semiconductor to metal phase is involved. The structural PT from O to M1″ phase is a typical Peierls PT or pseudo Mott PT rather than actual Mott PT within our DFT+U calculations.

II. COMPUTATIONAL METHODS

Our DFT calculations were carried out with projector augmented wave pseudo-potentials (PAW) at generalized gradient approximation (GGA) through Vienna *ab initio* simulation package (VASP) [36–39]. The Brillouin zone integrations were chosen as the special $5 \times 7 \times 6$ (M1) and $10 \times 10 \times 10$ (R) k-point sampling of the Monkhorst-Pack type, respectively. The kinetic energy cutoff of 600 eV was found to ensure the total energy convergence to 10^{-6} eV/atom. The geometric structure optimizations were performed using the conjugated-gradient minimization scheme until the maximum residual force on each atom was less than 0.01 eV/Å. All band gaps were calculated with GGA+U method (with an effective $U = 3.30$ eV) [28], which is not sensitive to pressurization from the results of our structural studies. Under ambient pressure, monocline VO_2 (M1) is a semiconductor phase with a theoretical band gap of 0.68 eV. In order to describe the strongly correlated effect as accurately as possible in $3d$ transition metal elements, DFT+U method is usually required to predict band gap more accurately.

The on-site Hubbard interaction can be estimated with $U = E_{gap} + (B_1 + B_2)/2$ [5] in which B_1 (B_2) is bandwidth of the upper (lower) Hubbard band and E_{gap} is the experimental band gap (0.60 eV [40]) of bulk VO_2. Our theoretical U value should be 1.30 eV ($B_1 = 0.87$ eV, $B_2 = 0.53$ eV) within this estimation. Apparently, the effective on-site Coulomb interaction ($U = 3.30$ eV) used in our calculation is much greater than that theoretical estimation (1.30 eV). The intersite Coulomb repulsion V between electrons is not taken into account in the present DFT + U calculations. However, the main aim of U within our DFT + U calculations is to increase the energy gap to reach the experimental value while its main effect of V is to increase the bonding-antibonding splitting [41], so the excessive portion ($2.00 = 3.30$–1.30 eV) in the U parameter may generally represents the impact of the V parameter on the energy band gap. The influence of the V parameter ($\sim$2.00 eV) on the energy band gap is greater than that of the U parameter, which is consistent with the predictions of previous dynamical mean-field theory (DMFT) theory [22].

M1 and R phases are experimentally nonmagnetic state and paramagnetic state with a weak local magnetic moment [42,43], respectively. Moreover, Previous theoretical studies [43–45] and our calculations [46] (TABLE S-1 in the Supplemental Material) show that the relative stability of R and M1 phase will be the wrong order in the spin-polarization calculations. So the spin-unpolarization calculations were finally chosen to simulate various geometrical and electronic structures. In the last decade many publications have shown that a description of the dynamical correlations is important such as with DMFT or its cluster extensions. Unfortunately, different calculations by state-of-the-art DFT+DMFT methods do not even agree with a unanimous view of the M1 monoclinic phase. Specifically, M1 has been regarded from time to time as a correlation-assisted Peierls insulator [20,47], or vice versa, as a Peierls-assisted Mott insulator [48], or finally as a genuine Mott insulator [23,49,50]. In our calculations, a consistent computational functional (DFT+U with a nonmagnetic solution) is greatly important to yield a rational and continual evolution of geometrical and electronic structure during MIT.

In addition, it has been shown that the Heyd-Scuseria-Ernzerhof (HSE) hybrid functional can successfully reproduce the band gap for the M1 phase [51], however, it incorrectly predicts an antiferromagnetic ground state for all three phases (namely, M1, M2, and R) of VO_2 [45]. Thus, the choice of using DFT+U over more computationally demanding hybrid functionals is a result of following three considerations. First, the HSE functional has no advantages over conventional DFT+U functionals for various energy descriptions. Second, DFT+U can also predict the band gap equally well at a greatly reduced computational cost. Third, the HSE functional for structural optimization at various pressures is extremely expensive in computation. In particular, phonon calculations using HSE functionals for many structures are prohibitively time consuming. All these benefits have been described in the previous theoretical study [29]. The phonon dispersions were computed based on the supercell approach using the PHONOPY code [52] with $2 \times 2 \times 2$ supercells for the M1, M1′, M1″, O, and X structures.

III. RESULTS AND DISCUSSION

A. M1-M1′/M1″ PT

Our theoretical lattice constant c tends to decrease linearly with increasing pressure, and theoretical lattice constants a and b show anomalous changes at 15 GPa with a clockwise (M1″) and anticlockwise (M1′) rotations (viewed along the c axis) of oxygen octahedron similar to that of $CaCl_2$ as shown in Fig. 1(a) and Table S-2. The lattice constants a and b show opposite trends after the PT point owing to the different rotational directions of oxygen octahedron as shown

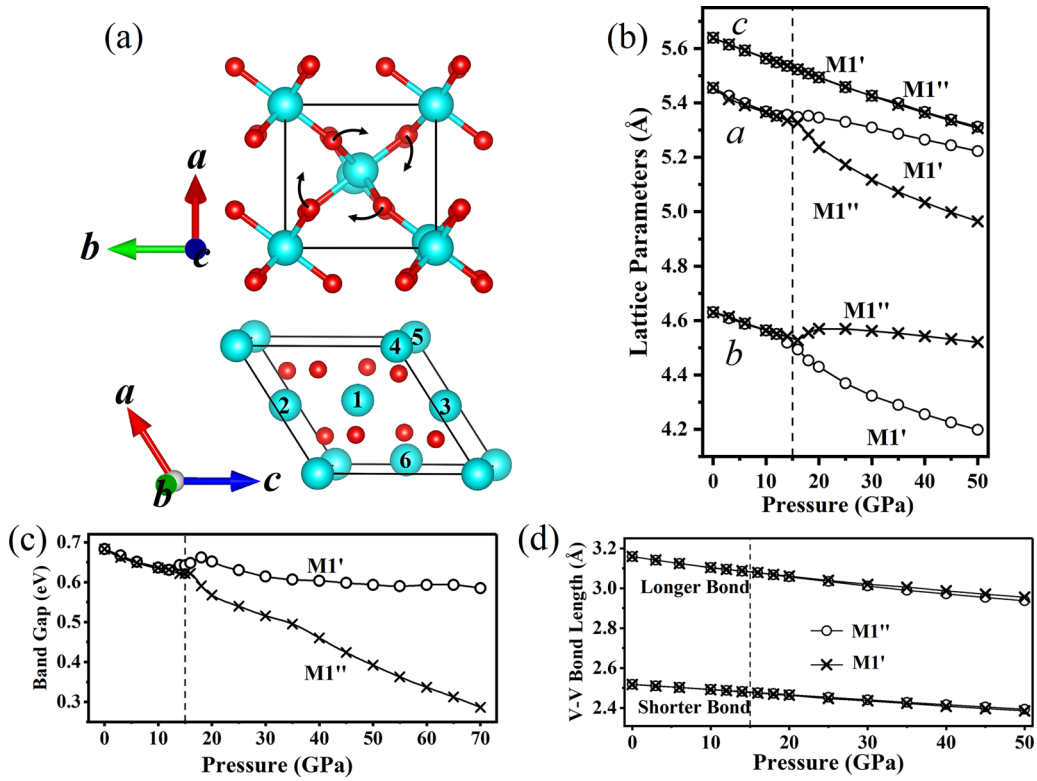

FIG. 1. (a) Rotation directions of oxygen octahedron from M1 to M1″ phase. Red and cyan spheres represent oxygen and vanadium atoms, respectively. ***a*/*b*/*c*** represent the primitive vectors of the crystal lattices. The numbers on the vanadium atoms in the figure are only used to describe the bond length and bond angle between specific vanadium atoms. (b) Pressure dependence of lattice constants of M1′ and M1″. (c) Pressure dependence of band gap for M1′ and M1″. (d) Evolution of V-V bond length of shorter and longer bonds in M1′ and M1″ phase. Dotted lines indicate the phase transition pressure at approximately 15 GPa.

in Fig. 1(b), where a decreases more rapidly while b decreases more slowly for M1″ phase, predicted by previous theoretical simulations [29].

Previous measured pressure-dependent resistivity [28,53] indicates a significant reduction of band gap with increasing pressure. Unlike the M1′ phase, which shows a nearly pressure-independent gap with approximately 0.6 eV, the M1″ phase shows a significant reduction of band gap with increasing pressure at high pressures as shown in Fig. 1(c). The calculated band gap of the M1″ phase starts to decrease quickly when pressure exceeds around 35 GPa and never closes even though the pressure reaches around 70 GPa. However, experimental band gap (as measured by pressure-dependent resistivity) starts to decrease at lower pressures and the gap closes at around 30 GPa [28]. Obviously, the M1″ phase is definitely not the metal phase observed in the experimental measurements [28,53] since the appearance of the metal phase should be inevitably accompanied by an averaging of V-V atomic bond. Although the bonds between V-V decrease with increasing pressure as shown in Fig. 1(d), the difference between shorter and longer bonds always exists. It is unimaginable that only the rotation of the V-O octahedron during the pressurization will lead to the averaging of the V-V bond. A new PT mechanism should be introduced to understand the metallization effect [28,53].

In the M1 phase, the dimerization and tilting of the V-V pairs result in two important effects. Within the Goodenough's picture [11,13], the tilting is responsible for the energy shift between the a_{1g} band and the e_g doublet. However, the tilting of V-V pairs is always accompanied by the reduction of all V-V bond lengths and unit volume in order to reduce potential energy during the M1 → M1″ PT. Moreover, if the tilting melts and then enlarges the angle of V_2-V_1-V_3 bond without the change of the V_2-V_1 bond length before the dedimerization, the energy gap and spectral weight also change slightly. So we will no longer discuss tilting of the V-V pairs separately in the following paragraphs.

Since it is well known that the low-energy electronic properties of VO_2 are dominated by the behavior of V d states, it is rather puzzling that opposite oxygen rotational distortions in the M1′ and M1″ phases can have such drastically different effects on the electronic properties. The pressure-induced reduction of band gap in the M1″ phases was explained in terms of dedimerization and dezigzagging of the V-V dimers owing to oxygen rotation [29]. Actually, the valence band maximum (VBM) of vanadium dioxide is contributed by the hybrid orbital of $2p$ orbitals of the oxygen atoms and $3d$ orbitals of the vanadium atoms, while the conduction band minimum (CBM) is mainly contributed by the $3d$ orbitals of the vanadium atoms as shown in Fig. S-1. The band gaps in the M1′ and M1″ structures should be closely related to the overlap energies between vanadium atoms at the CBM and vanadium (or oxygen) atoms at the VBM based on the tight-binding theory in solid state physics for energy bands,

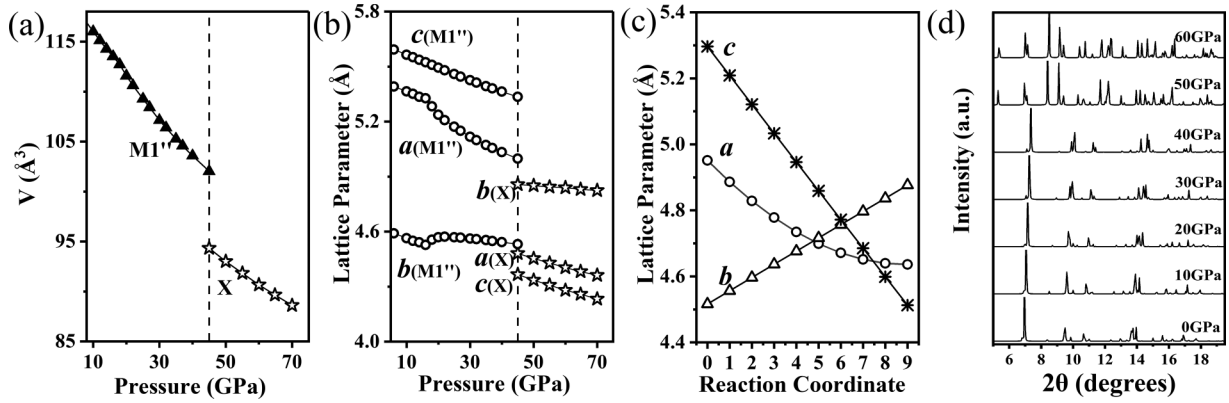

FIG. 2. (a) Pressure dependence of volume of X and M1″ phase. Dotted lines indicate the phase transition pressure at approximately 45 GPa. (b) Pressure dependence of lattice parameters of M1″ and X-phase. (c) Evolution of the lattice parameters with shuffling of the middle-layer V atoms along the most probable path under quasi static approximation. (d) Theoretical high-pressure powder XRD for M1″ and X phase vs pressure.

which decreases exponentially with those atomic separations [54]. Relatively longer lengths of V-V shorter bond in Fig. 1(d) and Fig. S-2(a) and V-O bond in Fig. S-2(b) clearly reveals that its band gap should be smaller in the M1″ configuration as shown Fig. 1(c). A decreasing band gap of M1′ and M1″ phase by uniaxial pressurization (a, b, and c crystal directions) were further calculated, however, the metallic phase or any new phase has not been theoretically obtained.

In addition, M1″ structures should have been actually observed in the experimental pressure-induced PT. Theoretical phonon calculations have indicated its dynamic stability owing to no negative frequency [29]. It is difficult to distinguish M1′ and M1″ structures through experimental x-ray diffraction (XRD) as shown in Fig. S-3(a-b) or Raman spectra, etc. However, there is a significant difference in the conductivity for M1′ and M1″ structures. If the M1′ phase experimentally observed was indeed M1′ structure, its conductivity would drop sharply and exhibit discontinuity at the intersection of M1′ and X as shown in Fig. S-4. However, there is no discontinuity in the conductivity measured in the experimental measurements [28], so we speculated that the M1′ phase observed in the experiments [28] is actually M1″ phase.

B. M1″/M1′-X PT

1. Evolution of geometrical structure for M1″/M1′-X PT

A baddeleyite structure ($P2_1/c$ space group, called as X phase) was obtained by shuffling those V atoms at the (002) crystal plane of crystal cell nearly along the [100] crystal direction for M1″ phase under approximately 45 GPa as shown in TABLE S-2 and Fig. S-5. The shuffling vector $\boldsymbol{r}$ equals $0.33\boldsymbol{a}_1 + 0.11\boldsymbol{a}_3$. The volume of M1″ phase decreases only by approximately 5% after the PT to X phase at 45 GPa as shown in Fig. 2(a). The baddeleyite structure holds a larger b lattice constant, and smaller a as well as c lattice constants relative to M1″ configuration as shown in Fig. 2(b). The experimental b lattice constant ($b = 9.686$ Å) [28] is too large to actually appear in the PT owing to only shuffling of some crystal plane, which may be the crystal cell parameters of twins. Half of that is likely to be the appropriate parameter, which is consistent with our theoretical prediction ($b = 4.872$ Å). Our theoretical diffraction peaks as shown in Fig. 2(d) appeared in regions of 2θ between 6° and 9° for the X phase are strongly supported by previous high-pressure powder XRD experimental measurements [28]. Their XRD measurements [28] revealed that the X phase starts at 34.3 GPa and become dominant at 55.3 GPa, which also supports our theoretical PT pressure.

The enthalpies of M1′ and M1″ intersect with that of X phase under approximately 45 GPa, indicating the X phase is more stable than M1′ and M1″ phase above 45 Gpa as shown in Fig. S-6(a). There is not any imaginary frequency in the theoretical phonon dispersion of the X phase as shown in Fig. S-6(b), which further reveal that our X phase is dynamically and thermodynamically stable state above 45 Gpa.

The energy barrier is 285 meV/VO_2 through the climbing image nudged elastic band method (CL-NEB) [55] with the shuffling of those V atoms at the (002) crystal plane of crystal cell nearly along the [100] crystal direction for the most probable path under quasi static approximation as shown in Fig. 3(a). It represents a shear stress of at least 15–16 Gpa should be provided if the PT from M1″ to X phase is successfully driven at a certain volume (corresponding to the 45 Gpa). This is why the shear stress must be applied along [001] crystal direction instead of only hydrostatic pressure (45 Gpa) to drive PT from M1″ to X phase in our simulations.

Certainly, shuffling those V atoms at the (002) crystal plane of crystal cell along the [100] crystal direction for M1′ phase also leads to our X phase. Its moving path is more tortuous and distant for V atoms from M1′ to X structure. Moreover, M1′ has a smaller b lattice constant, however, the PT products (X phase) require a larger b lattice constant. Therefore, it is more difficult for M1′ phase to transform into X phase under high pressure which can be understood from the Figs. 1(b), 2(c), and 3(a). It is actually experimentally possible to achieve structural PT from M1′ to X under higher pressure if the pressurization time is long enough and the pressure is large enough. The dispersion of various experimental PT pressures [30,32] may be related to the PT initiators (M1′ or M1″).

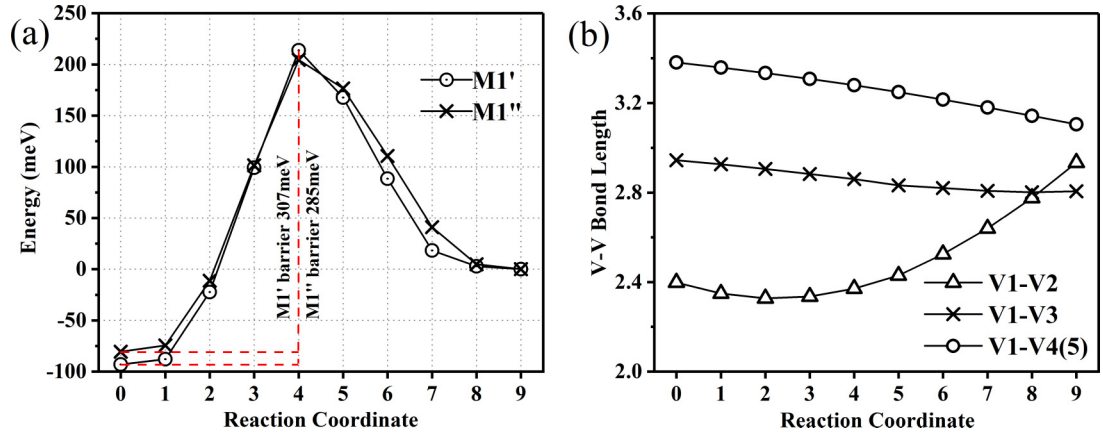

FIG. 3. (a) Potential energy curves from M1′ and M1″ of VO_2 to X phase under 45 GPa. (b) Evolution of V-V bond length for shorter and longer bonds from M1″ to X phase under 45 GPa.

2. *Evolution of electronic structure for M1″/M1′-X PT*

The evolutions of electronic and geometrical structures with shuffling those V atoms at the (002) crystal plane of crystal cell nearly along the [100] crystal direction for M1″ phase were shown in Figs. 3(b) and 4. From the M1″ state (band gap 0.45 eV) to the eighth configuration (band gap 0.08 eV), their geometrical structure, band structure, and local partial density of states (LDOS) are very similar as shown in Figs. 4(a), 4(a′), and 4(a″). All configurations are semiconductors with nonzero energy gap. At this stage, the original V_2-V_1-V_3 chemical bond along the [001] direction breaks, and then all V-V chemical bond lengths are averaged as shown in Fig. 3(b). The band gap decreases gradually and no PT of electronic structure is involved.

When those V atoms at the (002) crystal plane of crystal cell continuously shuffle nearly along the [100] crystal direction to the ninth configuration (X phase). It actually becomes a semimetal with negative pseudoenergy gap (band gap −0.03 eV) as shown in Figs. 4(b), 4(b′), and 4(b″). At this stage, the averaging of all V-V chemical bond lengths is not yet complete, which is why the X phase is a semi metallic rather than a metallic phase. It is only a geometrical structural PT and the gradual closing of the band gap is always accompanied by the averaging of V-V atomic separations.

During the PT from M1″ to X phase, only the band gap decreases gradually, and with the reconstruction of atomic chemical bond. It is a typical reconstructed and martensiticlike PT, and no PT of electronic structure from semiconductor to metal phase is involved.

Changing the U value only changes the theoretical pressure in the PT and energy gap of the X phase as shown in Fig. S-7, however, it cannot change the properties of the semimetal and PT path.

Previous pressure dependence of electrical resistivity of VO_2 at ambient temperature indicated that a dramatic reduction in resistivity with increasing pressure by more than five orders of magnitude, from 10^{-2} Ωm (at 5.3 GPa) to 10^{-6} Ωm (at 61.4 GPa) [28]. The experimental conductivity of the X

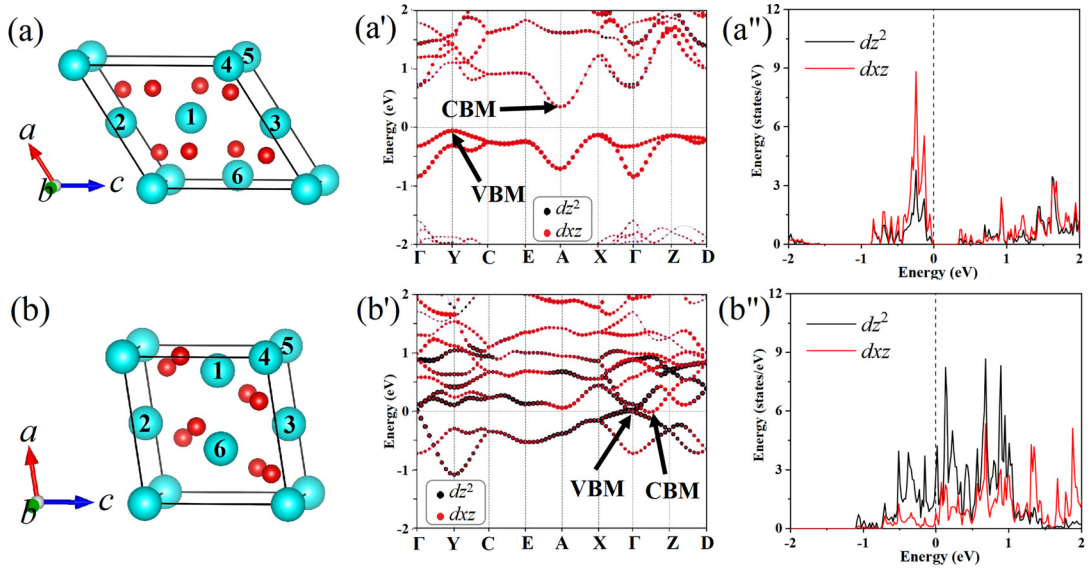

FIG. 4. (a/a′/a″)-(b/b′/b″) Geometrical structure, energy band structure, and LDOS during PT. a/a′/a″ figures represent M1″, b/b′/b″ figures represent the ninth configuration (X phase).

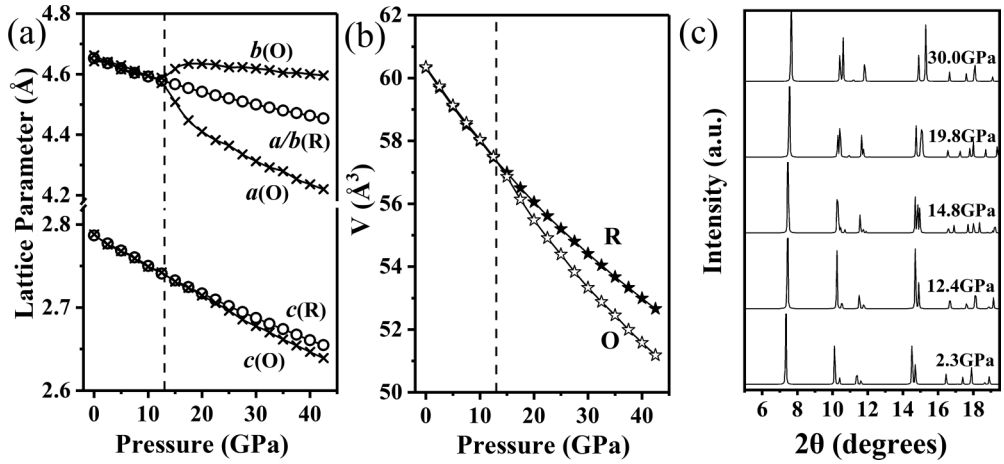

FIG. 5. (a) Uniaxial-external pressure dependence of lattice constants of R and O phase along the [100] crystal direction. Dotted lines indicate the phase transition pressure at approximately 13 GPa. (b) Uniaxial-external pressure dependence of lattice volumes of R and O phase along the [100] crystal direction. (c) Theoretical high-pressure powder XRD for R and O phases.

crystal phase is within the conductivity range of a semi metal [56], which is well agreement with our semimetal calculations for X phase. In the calculations of conductivity and carrier concentration, the electron relaxation time (τ) is very time consuming with Boltzmann theory [57]. Therefore, for complex multistructure PT or high-throughput operations, a constant relaxation time ($\tau = 10$) approximation is usually used [18]. Our theoretical conductivity monotonically and continuously increases with increasing pressure as shown in Fig. S-4, and finally reaches a saturation value for X phase. The whole trend is completely consistent with the experimental measurement [28].

In the last decade the DMFT has made great progress [9,20,22,24,41,48,58,59]. DMFT generally estimates more properly the role of magnetic ordering in VO_2, i.e., the ground state of the system should not be metallic if the lattice distortions are properly included. The same energy band as DFT+U should be obtained even with DMFT. If there was any difference in pressure dependence of conductivity between DMFT and DFT+U, it only should lie in the fact that the semimetal phase obtained from the DFMT maybe appear earlier (or later) than our theoretical PT pressure, which means the steeper (or gentle) curve for pressure dependence of conductivity and a saturation of conductivity value reached under lower (or higher) pressure from M1″ to X phase. However, the experimental conductivity reaches saturation only when external pressure exceeds approximately 42 GPa [31], slightly greater than our theoretical pressure (40 GPa) as shown in Fig. S-4. Obviously, like DMFT, our calculations within DFT+U also can reasonably describe the PT behavior even though it does not directly contain the intersite Coulomb interactions.

C. R-O PT

Uniaxial stressing of the R metal phase along [100] or [010] crystal direction leads to the $CaCl_2$-type orthogonal metal phase (O phase, space group No. 58, *Pnnm*) at around 13 GPa as shown in Figs. 5(a) and S-8, which is a stress-driven type of second-order distortion resulting from a clockwise ($a < b$ in O-phase, [100] crystal direction for uniaxial external stress) or anticlockwise ($a > b$ in the O phase, along [010] crystal direction for uniaxial external stress) rotation around the c axis (viewed along the c axis) for the distorted VO_6 octahedron. Compared with R phase, a- and b-lattice parameters of O phase split into opposite trends as shown in Fig. 5(a). With increasing pressure, the c-lattice parameters and volume decrease more rapidly, and by 40 GPa, the O-phase volume decreases by approximately 0.3% compared with the R-phase. Our theoretical XRD diffraction pattern of the R-phase with increasing pressure shows some splitting and broadening of diffraction peaks around 13 GPa and generates new diffraction peaks in regions of 2θ between 10° and 11° as shown in Fig. 5(c) which strongly supported by previous high-pressure powder XRD experimental measurements [28].

The enthalpies of R intersect with that of the O phase at around 18.5 GPa, indicating that the O phase is more stable than R phase above 18.5 GPa pressure as shown in Fig. S-9(a). There is not any imaginary frequency in the theoretical phonon dispersion of the O phase as shown in Fig. S-9(b), which further reveals that our O phase is a dynamically and thermodynamically stable state above 18.5 GPa at room temperature. In the early stage of PT, the cell volume does not decrease significantly while the distorted VO_6 octahedrons have larger rotation around the c axis. Larger rotation of those distorted VO_6 octahedrons lead to decrease significantly of internal energy, so there exists a difference in PT point from the calculations of enthalpy [18.5 GPa in Fig. S-9(a)] and internal energy [13 GPa in Fig. 5(a)]. There is not any energy barrier using the CL-NEB method [55] with the rotation around the c axis for the oxygen octahedral structure for the most probable path under quasistatic approximation under approximately 20 GPa as shown in Fig. S-10(a). No energy barrier also reveals that a small pressure or thermal fluctuation after volume compression of 0.3% can bring out R → O PT.

Both R [31] and O phases are metallic phases as shown in Fig. S-10(b)-(c). The structural PT of R → O resembles M1 → M1′/M1″ PT. They are only geometric PTs caused by the rotation of the V-O octahedron around the c axis without the transformation of electronic structure. The only difference

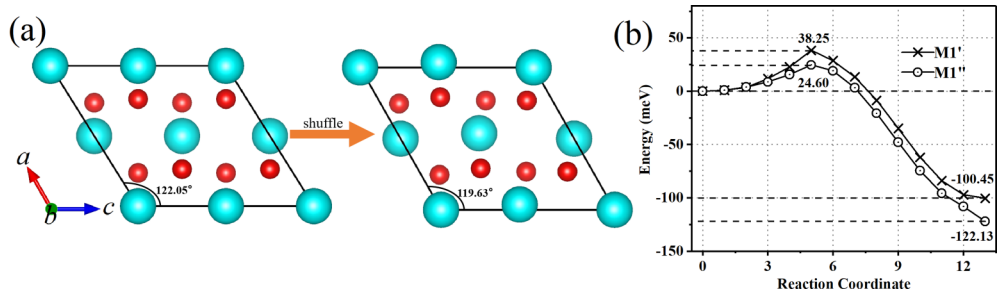

FIG. 6. (a) Shear-stress-driven structural PT from the O to M1″ phase. (b) Potential energy curves from O to M1′/M1″ phase under 20 GPa.

is that M1 → M1′/M1″ is insulator → insulator PT while R → O is metal → metal PT.

D. O-X PT

1. Evolution of geometrical structure for O-X PT

When we studied the various possible transition paths from the O phase to the X phase, we found that its theoretical energy barrier is too large to directly realize this PT. However, the energy barriers from O to M1′ or M1″ phase are only 25 and 38 meV/VO_2 under the shear stress of 20 GPa along the [001] crystal direction, respectively, as shown in Figs. 6(a) and 6(b). For a potential barrier of 20 ∼ 40 meV/VO_2, only a few GPa of pressure can theoretically result in PT, which perfectly explains that after a pressure greater than 13–15 GPa, there is only a thermally induced PT between the O phase and the X phase in the experimental pressure-temperature phase diagram [31]. The energy barriers from M1′ or M1″ to O phase are 139 and 147 meV/VO_2, respectively. From the ideal gas model [60,61], this is roughly equivalent to the potential barrier that can be overcome in the thermally induced PT at approximately 460 ∼ 487 K on heating. The O phase always exists above 360 K in the experimental pressure-temperature phase diagram [31], also reflects the existence of such a theoretical energy barrier.

So R → O → M1′/M1″ → X is the most likely path for pressurizing the rutile R phase to the semimetallic X phase. A sketch of the pressure-temperature phase diagram is presented as shown in Fig. S-11(a). Its main part of our sketch comes from the reference [31]. The enthalpies of O are always higher than those of M1′/M1″ phase as shown in Fig. S-11(b), indicating the M1′/M1″ phase is invariably more stable than O phase.

2. Evolution of electronic structure for O-M1″ PT

The evolutions of the longer and shorter V-V bond with shuffling those V atoms at the (002) crystal plane of crystal cell along the [10-1] crystal direction for O phase were shown in Fig. 6 and Fig. S-12. The shuffling vector $\boldsymbol{r}$ equals $0.03\boldsymbol{a}_1 - 0.03\boldsymbol{a}_3$. From the O phase to fifth configuration, their geometrical structure, band structure, and LDOS are very similar as shown in Fig. 7 (a-a′) which illustrates that all of them are metal phase and the V-V spacing remains nearly constant as shown in Fig. S-12. At this stage, only geometrical distortion occurs, and no PT of electronic structure is involved even though Coulomb repulsion between electrons is always present.

When those V atoms at the (002) crystal plane of crystal cell continuously shuffle along the [10-1] crystal direction to the tenth configuration, the difference in longer and shorter V-V bond lengths tends to increase as shown in Fig. S-12. They become indirect semimetal phase with zero pseudoenergy gap as shown in Fig. 7 (b′-b″). At this stage, the electrons can always jump down rather than jump up to the CBM under thermal fluctuation to form conductive carriers owing to electrons at VBM with higher potential energy than those at CBM. The electron jumping does not require additional energy from Coulomb repulsion between electrons even though it is always present [18]. So there is always a Peierls PT or called as pseudo- Mott PT within our band energy scheme in DFT+U calculations because Coulomb repulsion between electrons is always present and not needed to make this work.

From tenth (zero pseudo energy gap) to 13th (M1″, band gap 0.45 eV) configuration, the band gap increases gradually and the difference in longer and shorter V-V bond lengths becomes larger as shown in Fig. S-12. New dimerization of the V_1-V_2 dimers along [001] crystal direction appears as shown in Fig. 6(a). At this stage, only geometrical distortion occurs, and no PT of electronic structure is involved.

The discussion above can be briefly summarized as follows: The structural PT path from O → M1″ phase is generally divided into three stages. At first and third stages, there is not any electronic structural PT and it is only involved in metal → metal or semiconductor → semiconductor "distortion" or minimal change rather than PT even though strong Coulomb repulsion between electrons can make a large number of electrons jump up from lower bands to higher bands. The electronic structural PT only occurs in the second stage in which the band gap is zero or negative value. Thermal fluctuations are sufficient to drive electrons to jump down to CBM even though the Coulomb repulsion between electrons is always present and can also make a large number of electrons to jump upward. Previous studies [19–25] suggested that the cooperation of Mott correlation and Peierls distortion play an important role in the PT at the same time, which strongly support our calculations. However, Coulomb repulsion between electrons cannot cause the electronic structural PT to happen properly within our DFT+U calculations.

DMFT with a two-site cluster model and x-ray absorption spectroscopies [62] predicted the symmetry switch of frontier orbitals in the PT from the M1 to R phase. Obviously, the frontier orbitals $d_{x2\text{-}y2}$ at E_F of O phase is different from that (d_{xz} at VBM) of M1″ phase as shown in Fig. 7 which also indicates that our calculations are reliable.

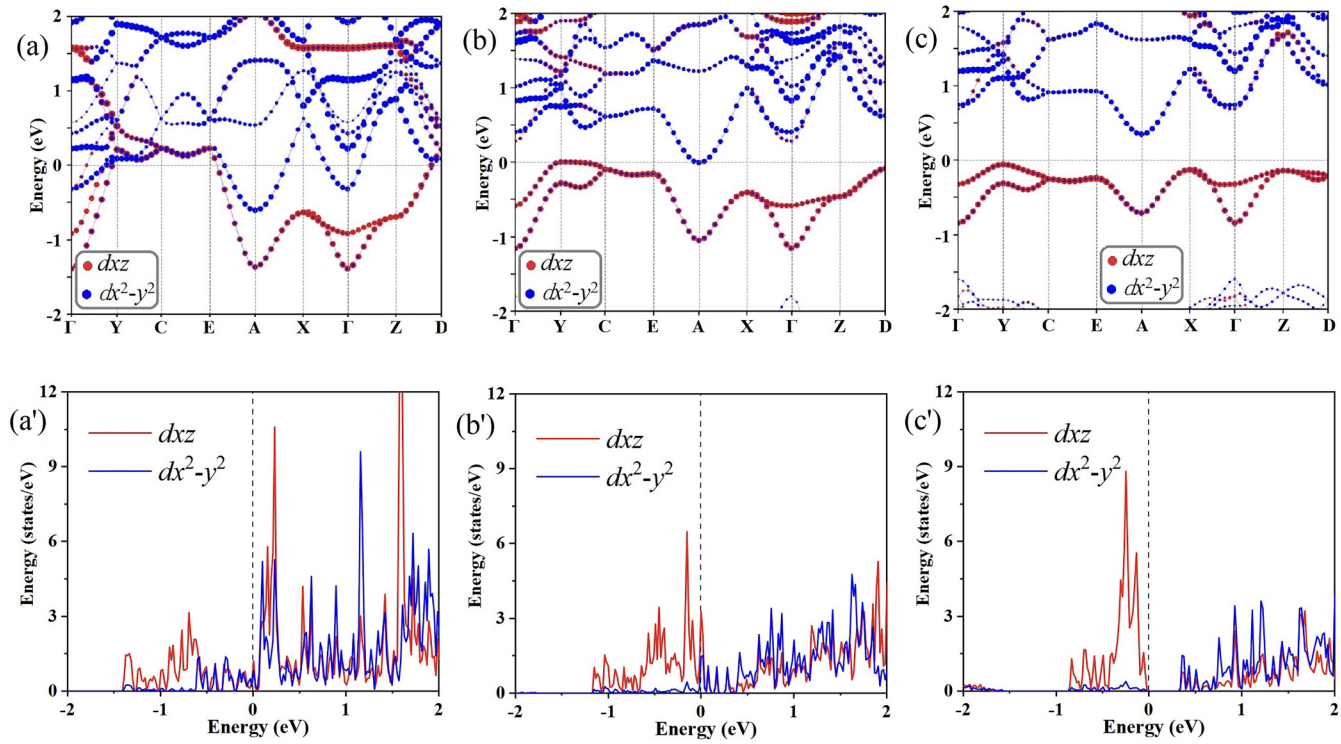

FIG. 7. (a/a′)-(c/c′) Energy band structure, and LDOS during PT. a/a′ figures represent O and first–ninth configurations, b/b′ figures represent the tenth configuration, and c/c′ figures represent the 11th–13th configurations.

IV. CONCLUSION

The evolutions of structural and electronic properties of VO_2 under pressure were studied with first-principles calculations. We found the M1 → M1″ → X and R → O → M1″ → X paths are the most likely routes under pressure at room and higher temperature. Both PT paths from the semiconductor M1 → semiconductor M1″ → semimetal X phase and from metal R → metal O phase only involve geometrically structural PT. The structural PT path from metal O → semiconductor M1″ phase is a typical Peierls PT or pseudo-Mott PT within our DFT+U treatments. Its electronic structural PT only occurs in the middle stage in which the band gap is zero or a negative value. Thermal fluctuations are sufficient to drive electrons to jump down to CBM even though the Coulomb repulsion between electrons is always present and works, which means that Coulomb repulsion between electrons always works, however, the electronic PT occurs in a stage where Coulombic interaction is not required to work within our DFT+U treatments.

During the pressurization of the M1 phase, it will transform into two nearly degenerate intermediate phases of M1′ and M1″. The M1″ phase has a significantly lower band gap (no zero band gap) owing to its relatively longer length of V-V shorter bond and V-O bond. During the PT from the M1″ to the X phase, those V atoms at the (002) crystal plane of crystal cell will shuffle nearly along the [100] crystal direction as volume pressurization, while the averaging of V-V spacing occur and the band gap gradually decreases to zero or even a negative value. The gradual closing of the band gap is always accompanied by the averaging of V-V atomic separations. Uniaxial stressing of the metal R phase along the [100] or [010] crystal direction leads to the $CaCl_2$-type orthogonal metal phase (O phase, space group No. 58, *Pnnm*) which is a stress-driven type of second-order distortion resulting from a rotation around the *c* axis for the distorted VO_6 octahedron. And then upon cooling the O phase under high pressure, it will transform to M1″ and then the X phase. Those V atoms at the (002) crystal plane of crystal cell continuously shuffle along the [10-1] crystal direction from O phase to M1″ configuration, moreover the difference in longer and shorter V-V bond lengths tends to increase and new dimerization of the V-V dimers appears. The gradual opening of the band gap is invariably accompanied by the formation of dimerization of V-V atoms.

ACKNOWLEDGMENTS

This work was supported by the National Natural Science Foundation of China under Grants (No. 51872227 and 51572219).

[1] F. J. Morin, Oxides Which Show a Metal-to-Insulator Transition at the Neel Temperature, Phys. Rev. Lett. **3**, 34 (1959).

[2] J. Cao, E. Ertekin, V. Srinivasan, W. Fan, S. Huang, H. Zheng, J. W. Yim, D. R. Khanal, D. F. Ogletree, J. C. Grossman, and J. Wu, Strain engineering and one-dimensional organization

of metal-insulator domains in single-crystal vanadium dioxide beams, Nat. Nanotechnol. **4**, 732 (2009).

[3] S. Wall, S. Yang, L. Vidas, M. Chollet, J. M. Glownia, M. Kozina, T. Katayama, T. Henighan, M. Jiang, T. A. Miller, D. A. Reis, L. A. Boatner, O. Delaire, and M. Trigo, Ultrafast disordering of vanadium dimers in photoexcited VO_2, Science **362**, 572 (2018).

[4] M. Nakano, K. Shibuya, D. Okuyama, T. Hatano, S. Ono, M. Kawasaki, Y. Iwasa, and Y. Tokura, Collective bulk carrier delocalization driven by electrostatic surface charge accumulation, Nature (London) **487**, 459 (2012).

[5] A. Zylbersztejn and N. F. Mott, Metal-insulator transition in vanadium dioxide, Phys. Rev. B **11**, 4383 (1975).

[6] T. M. Rice, H. Launois, and J. P. Pouget, Comment on "VO_2: Peierls or Mott-Hubbard? A View from Band Theory," Phys. Rev. Lett. **73**, 3042 (1994).

[7] A. Cavalleri, T. Dekorsy, H. H. W. Chong, J. C. Kieffer, and R. W. Schoenlein, Evidence for a structurally-driven insulator-to-metal transition in VO_2: A view from the ultrafast timescale, Phys. Rev. B **70**, 161102 (2004).

[8] M. M. Qazilbash, M. Brehm, B. G. Chae, P. C. Ho, G. O. Andreev, B. J. Kim, S. J. Yun, A. V. Balatsky, M. B. Maple, F. Keilmann, H. T. Kim, and D. N. Basov, Mott transition in VO_2 revealed by infrared spectroscopy and nano-imaging, Science **318**, 1750 (2007).

[9] O. Nájera, M. Civelli, V. Dobrosavljević, and M. J. Rozenberg, Resolving the VO_2 controversy: Mott mechanism dominates the insulator-to-metal transition, Phys. Rev. B **95**, 035113 (2017).

[10] T. J. Huffman, C. Hendriks, E. J. Walter, J. Yoon, H. Ju, R. Smith, G. L. Carr, H. Krakauer, and M. M. Qazilbash, Insulating phases of vanadium dioxide are Mott-Hubbard insulators, Phys. Rev. B **95**, 075125 (2017).

[11] J. B. Goodenough, Direct cation–cation interactions in several oxides, Phys. Rev. **117**, 1442 (1960).

[12] D. Adler and H. Brooks, Theory of semiconductor-to-metal transitions, Phys. Rev. **155**, 826 (1967).

[13] J. B. Goodenough, The two components of the crystallographic transition in VO_2, J. Solid State. Chem. **3**, 490 (1971).

[14] R. M. Wentzcovitch, W. W. Schulz, and P. B. Allen, VO_2: Peierls or Mott-Hubbard? A View from Band Theory, Phys. Rev. Lett. **72**, 3389 (1994).

[15] V. Eyert, The metal-insulator transitions of VO_2: A band theoretical approach, Ann. Phys. **514**, 650 (2002).

[16] M. M. Qazilbash, A. A. Schafgans, K. S. Burch, S. J. Yun, B. G. Chae, B. J. Kim, H. T. Kim, and D. N. Basov, Electrodynamics of the vanadium oxides VO_2 and V_2O_3, Phys. Rev. B **77**, 115121 (2008).

[17] J. M. Booth and P. S. Casey, Anisotropic Structure Deformation in the VO_2 Metal-Insulator Transition, Phys. Rev. Lett. **103**, 086402 (2009).

[18] J. Y. Miao, W. X. Wang, Z. Y. Jiang, X. D. Zhang, J. M. Zheng, and A. Du, A theoretical study on pseudo Mott phase transition of vanadium dioxide, Phys. Chem. Chem. Phys. **25**, 759 (2022).

[19] D. Paquet and P. Leroux-Hugon, Electron correlations and electron-lattice interactions in the metal-insulator, ferroelastic transition in VO_2: A thermodynamical study, Phys. Rev. B **22**, 5284 (1980).

[20] S. Biermann, A. Poteryaev, A. I. Lichtenstein, and A. Georges, Dynamical Singlets and Correlation-Assisted Peierls Transition in VO_2, Phys. Rev. Lett. **94**, 026404 (2005).

[21] M. W. Haverkort, Z. Hu, A. Tanaka, W. Reichelt, S. V. Streltsov, M. A. Korotin, V. I. Anisimov, H. H. Hsieh, H. J. Lin, C. T. Chen, D. I. Khomskii, and L. H. Tjeng, Orbital-assisted Metal-Insulator Transition in VO_2, Phys. Rev. Lett. **95**, 196404 (2005).

[22] W. H. Brito, M. C. Aguiar, K. Haule, and G. Kotliar, Metal-Insulator Transition in VO_2: ADFT+DMFT Perspective, Phys. Rev. Lett. **117**, 056402 (2016).

[23] D. Plašienka, R. Martoňák, and M. C. Newton, *Ab initio* molecular dynamics study of the structural and electronic transition in VO_2, Phys. Rev. B **96**, 054111 (2017).

[24] F. Grandi, A. Amaricci, and M. Fabrizio, Unraveling the Mott-Peierls intrigue in vanadium dioxide, Phys. Rev. Res. **2**, 013298 (2020).

[25] V. Jonsson, L. Piazza, M. Månsson, J. Weissenrieder, O. Tjernberg, S. Khartsev, Y. Sassa, D. G. Mazzone, N. Gauthier, M. Muntwiler, C. S. Ong, D. Iuşan, P. Thunström, and O. Eriksson, Photoelectron dispersion in metallic and insulating VO_2 thin films, Phys. Rev. Res. **3**, 033286 (2021).

[26] E. Arcangeletti, L. Baldassarre, D. Di Castro, S. Lupi, L. Malavasi, C. Marini, A. Perucchi, and P. Postorino, Evidence of a Pressure-Induced Metallization Process in Monoclinic VO_2, Phys. Rev. Lett. **98**, 196406 (2007).

[27] C. Marini, L. Baldassarre, M. Baldini, A. Perucchi, D. Di Castro, L. Malavasi, S. Lupi, and P. Postorino, Evidence for a monoclinic metallic phase in high-pressure VO_2, High Press Res. **30**, 55 (2010).

[28] L. Bai, Q. Li, S. A. Corr, Y. Meng, C. Park, S. V. Sinogeikin, C. Ko, J. Wu, and G. Shen, Pressure-induced phase transitions and metallization in VO_2, Phys. Rev. B **91**, 104110 (2015).

[29] H. He, H. Gao, W. Wu, S. Cao, J. Hong, D. Yu, G. Deng, Y. Gao, P. Zhang, H. Luo, and W. Ren, Phonon instability and pressure-induced isostructural semiconductor-semimetal transition of monoclinic VO_2, Phys. Rev. B **94**, 205127 (2016).

[30] H. Zhang, Q. Li, B. Cheng, Z. Guan, R. Liu, B. Liu, Z. Liu, X. Li, T. Cui, and B. Liu, The pressure-induced metallization of monoclinic vanadium dioxide, RSC Adv. **6**, 104949 (2016).

[31] Y. Chen, S. Zhang, F. Ke, C. Ko, S. Lee, K. Liu, B. Chen, J. W. Ager, R. Jeanloz, V. Eyert, and J. Wu, Pressure-temperature phase diagram of vanadium dioxide, Nano Lett. **17**, 2512 (2017).

[32] Q. Li, H. Zhang, C. Lin, F. Tian, J. S. Smith, C. Park, B. Liu, and G. Shen, Pressure-induced phase transitions and insulator-metal transitions in VO_2 nanoparticles, J. Alloys Compd. **709**, 260 (2017).

[33] M. Mitrano, B. Maroni, C. Marini, M. Hanfland, B. Joseph, P. Postorino, and L. Malavasi, Anisotropic compression in the high-pressure regime of pure and chromium-doped vanadium dioxide, Phys. Rev. B **85**, 184108 (2012).

[34] J. M. Braun, H. Schneider, M. Helm, R. Mirek, L. A. Boatner, R. E. Marvel, R. F. Haglund, and A. Pashkin, Ultrafast response of photoexcited carriers in VO_2 at high-pressure, New J. Phys. **20**, 083003 (2018).

[35] S. L. Dudarev, G. A. Botton, S. Y. Savrasov, C. J. Humphreys, and A. P. Sutton, Electron-energy-loss spectra and the structural stability of nickel oxide: An LSDA+U study, Phys. Rev. B **57**, 1505 (1998).

[36] P. E. Blöchl, Projector augmented-wave method, Phys. Rev. B **50**, 17953 (1994).

[37] J. P. Perdew, K. Burke, and M. Ernzerhof, Generalized Gradient Approximation Made Simple, Phys. Rev. Lett. **77**, 3865 (1996).

[38] G. Kresse and J. Furthmüller, Efficiency of *abinitio* total energy calculations for metals and semiconductors using a plane-wave basis set, Comput. Mater. Sci. **6**, 15 (1996).

[39] G. Kresse and J. Furthmüller, Efficient iterative schemes for *ab initio* total-energy calculations using a plane-wave basis set, Phys. Rev. B **54**, 11169 (1996).

[40] H. W. Verleur, A. S. Barker, and C. N. Berglund, Optical properties of VO_2 between 0.25 and 5 eV, Phys. Rev. **172**, 788 (1968).

[41] R. C. Juliano, A. S. de Arruda, and L. Craco, Coexistence and competition of on-site and intersite Coulomb interactions in Mott-molecular-dimers, Solid State Commun. **227**, 51 (2016).

[42] K. Takanashi, H. Yasuoka, Y. Ueda, and K. Kosuge, NMR studies of VO_2 and $V_{1-x}W_xO_2$, J. Phys. Soc. **52**, 3953 (1983).

[43] S. Chen, J. Liu, H. Luo, and Y. Gao, Calculation evidence of staged mott and peierls transitions in VO_2 revealed by mapping reduced-dimension potential energy surface, J. Phys. Chem. Lett. **6**, 3650 (2015).

[44] R. Grau-Crespo, H. Wang, and U. Schwingenschlögl, Why the Heyd-Scuseria-Ernzerhof hybrid functional description of VO_2 phases is not correct, Phys. Rev. B **86**, 081101 (2012).

[45] X. Yuan, Y. Zhang, T. A. Abtew, P. Zhang, and W. Zhang, VO_2: Orbital competition, magnetism, and phase stability, Phys. Rev. B **86**, 235103 (2012).

[46] See Supplemental Material, at http://link.aps.org/supplemental/10.1103/PhysRevB.108.064105 for details on Comparison of stability of spin-polarized and spin-unpolarized R and M1 phases.

[47] A. S. Belozerov, M. A. Korotin, V. I. Anisimov, and A. I. Poteryaev, Monoclinic M1 phase of VO_2: Mott-Hubbard versus band insulator, Phys. Rev. B **85**, 045109 (2012).

[48] C. Weber, D. D. O'Regan, N. D. Hine, M. C. Payne, G. Kotliar, and P. B. Littlewood, Vanadium Dioxide: A Peierls-Mott Insulator Stable Against Disorder, Phys. Rev. Lett. **108**, 256402 (2012).

[49] M. S. Laad, L. Craco, and E. Müller-Hartmann, Metal-insulator transition in rutile-based VO_2, Phys. Rev. B **73**, 195120 (2006).

[50] W. H. Brito, M. C. O. Aguiar, K. Haule, and G. Kotliar, Dynamic electronic correlation effects in NbO_2 as compared to VO_2, Phys. Rev. B **96**, 195102 (2017).

[51] V. Eyert, VO_2: A Novel View from Band Theory, Phys. Rev. Lett. **107**, 016401 (2011).

[52] T. Atsushi, O. Fumiyasu, and T. Isao, First-principles calculations of the ferroelastic transition between rutile-type and $CaCl_2$-type SiO_2 at high pressures, Phys. Rev. B **78**, 134106 (2008).

[53] X. Zhang, J. Zhang, F. Ke, G. Li, Y. Ma, X. Liu, C. Liu, Y. Han, Y. Ma, and C. Gao, Anomalous semiconducting behavior on VO_2 under high pressure, RSC Adv. **5**, 54843 (2015).

[54] C. Kittel and P. McEuen, *Introduction to Solid State Physics* (Wiley, New York, 2005), pp. 4441–4451.

[55] G. Henkelman, B. P. Uberuaga, and H. Jónsson, A climbing image nudged elastic band method for finding saddle points and minimum energy paths, J. Chem. Phys. **113**, 9901 (2000).

[56] A. H. Barajas-Aguilar, J. C. Irwin, A. M. Garay-Tapia, T. Schwarz, F. Paraguay Delgado, P. M. Brodersen, R. Prinja, N. Kherani, and S. J. Jimenez Sandoval, Crystalline structure, electronic and lattice-dynamics properties of $NbTe_2$, Sci Rep. **8**, 16984 (2018).

[57] J. Yang, H. Li, T. Wu, W. Zhang, L. Chen, and J. Yang, Evaluation of half-Heusler compounds as thermoelectric materials based on the calculated electrical transport properties, Adv. Funct. **18**, 2880 (2008).

[58] J. M. Tomczak, F. Aryasetiawan, and S. Biermann, Effective band structure in the insulating phase versus strong dynamical correlations in metallic VO_2, Phys. Rev. B **78**, 115103 (2008).

[59] O. Nájera, M. Civelli, V. Dobrosavljević, and M. J. Rozenberg, Multiple crossovers and coherent states in a Mott-Peierls insulator, Phys. Rev. B **97**, 045108 (2018).

[60] M. W. Zemansky, R. H. Dittman, and A. K. Chattopadhyay, *Heat and Thermodynamics*, 8th ed. (McGraw-Hill Education and China Machine Press, New York, 2015), p. 108.

[61] L. J. Xu and J. P. Huang, Robust one-way edge state in convection-diffusion systems, Europhys. Letts. **134**, 60001 (2021).

[62] T. C. Koethe, Z. Hu, M. W. Haverkort, C. Schussler-Langeheine, F. Venturini, N. B. Brookes, O. Tjernberg, W. Reichelt, H. H. Hsieh, H. J. Lin, C. T. Chen, and L. H. Tjeng, Transfer of Spectral Weight and Symmetry Across the Metal-Insulator Transition in VO_2, Phys. Rev. Lett. **97**, 116402 (2006).